


RESEARCH

Open Access



A heuristic model to evaluate the dielectric properties of human tissues at microwave band based on water and solid content

Marco Tannino^{1*} , Fabio Mangini¹, Lorenzo Dinia¹ and Fabrizio Frezza¹

*Correspondence:
marco.tannino@fondazione.
uniroma1.it

¹ Department of Information
Engineering, Electronics
and Telecommunications,
"Sapienza" University of Rome,
Rome, Italy

Abstract

At the molecular level, the body is composed, on average, of water for 62%, fat for 15%, 17% of protein, and 6% of minerals. In this work, we propose a heuristic methodology using hydration models as a base to realize an automatic and noninvasive procedure to estimate an ad hoc map of the complex dielectric permittivity of a generic human tissue in the frequency range of microwaves based on their solid and water content.

Keywords: Protein hydration, Human tissue permittivity, Water-of-hydration, Water property, Human model

Introduction

In silico models of the human body are increasingly used in dosimetry studies as well as in medical applications of electromagnetic fields. However, up to now, human body models are mostly derived from magnetic resonance imaging (MRI) through the segmentation of the different anatomical elements by expert teams of biologists and physicians [12, 61]. Moreover, the dielectric properties of tissues, to be used in combination with the geometrical models, are mostly obtained through ex vivo measurements [23, 27–29, 73]. Accordingly, this procedure limits the availability of human models, particularly useful in medical applications where the exact knowledge of the patient's anatomy and related electromagnetic properties would be of great benefit for the success of the treatment. As an example, in hyperthermia treatment planning (HTP) [47], simulations are carried out on the patients' anatomy to obtain the optimum hyperthermia protocol. However, the same should be performed in microwave thermal ablation, or microwave-based diagnostic applications, e.g., microwave tomography.

The relationship between water content and dielectric permittivity of human tissues and their electromagnetic interactions is well known [2, 4, 71, 79, 83]; however, even if a dielectric model of the human body was derived based on this assumption [60], an automatic tool was never devised. Several works were performed in the past to link the dielectric properties of the human body tissues with their water content [79, 83]. In these works, the dielectric properties of biological tissues were measured from audio

frequencies to microwaves, and some mathematical models were proposed to predict their values as a function of the frequency to understand the dielectric relaxation phenomena in tissues. Also, it is assumed that tissue's total water content belongs to two pools: 70% can be considered 'free water,' while 30% is the hydration water considered to be bound to the tissue's solid content and supposed to have the same dielectric properties of the dry protein [79, 83].

Proteins in aqueous solutions

Proteins are essential for life. These are the building blocks of cells and, virtually, part of every biological process. In organisms, proteins with biological functions usually exist in solution and many of their physical and functional properties are strongly influenced by the solvent. Therefore, it is vital to examine proteins within their common environment [89]. Since a large fraction of proteins exists in the aqueous intra-cellular or extra-cellular environment, the quantitative characterization of protein dynamics in aqueous solutions is essential for the understanding of living systems at a molecular level and many studies regard protein in aqueous solution in controlled conditions. Understanding the equilibrium existing between water and proteins within human tissues, thereby deducing a map of the tissues dielectric permittivity, is central to this study.

Water in hydrated proteins is often classified into three main groups: internal (or included) water, hydration water, and bulk (or free) water. The molecules of the water encounter highly heterogeneous protein surface sites, both for structure and electrostatics and characterization of the dynamics of the water molecules in the hydration layer. These aspects influence the dielectric properties of the hydration water. Both local curvature and chemical heterogeneity of the solute interface, e.g., clefts and pockets and hydrophobic or hydrophilic sites, influence the structure and dynamics of water. Internal water molecules occupy cavities within the protein and are present in most globular proteins [85, 88]. For most purposes, internal water molecules are best regarded as an integral part of the protein, even though they exchange with external water molecules, typically on a time scale of 0.1–10 μs [36, 37]. Forming up to four hydrogen bonds with neighbor molecules, reorientation of a water molecule is possible only when a sufficient number of hydrogen bonds are broken. The dielectric relaxation, in this way, is controlled by the lifetime τ_{HB} of H-bonds [43]. As a consequence of the presence of many factors influencing its dynamics, the hydration water within the hydration shell has a pronounced nonexponential character that reveals a broad distribution of reorientation times [85].

Many works have investigated the range of the hydration water and the geometry of the water compartments and their distribution around the hydrated macromolecules [38, 46, 48]. The water molecules next to the biomolecular interface, i.e., typically within 2.8–3.5 \AA generally define the first layer of water molecules in the hydration shell. A single water molecule occupies 2.8 \AA , and the molecules from 2.8 to 5.6 \AA are referred to as the second layer and so on [48]. Laage and co-workers have shown that the length-scale over which water adapts its bulk-water characteristics can vary between 2 and 10 hydration layers from the biomolecular surface depending on the parameters that have been under observation [48]. We have considered reasonable Persson and Halle's thesis [69] which uses a 5 \AA water-carbon cutoff, and a 4 \AA water-water cutoff has demonstrated

that the best assignment is for the first shell 4–5 Å thick, and the higher shells 2.8–4 Å tall. The different properties of water that are under the influence of the surface recover bulk-like characteristics at a different distance from the source of the perturbation. As a consequence, the experimental results need proper interpretation depending on the specificity of the property under observation [38].

Many works concluded that not only the hydration shell dynamics for all globular proteins can be rationalized by the same local topological and chemical factors but also, for many globular proteins, the hydration shell as a whole can have similar underlying distributions of reorientation times and, hence, similar overall dynamics. Fogarty and Laage performed molecular dynamics simulations of dilute aqueous solutions of four globular proteins, which cover a wide range of functions and molecular weights (from 9 to 59 kDa). They showed that all four proteins have very similar hydration shell dynamics, despite their wide range of sizes and functions, and differing secondary structures. They demonstrated that this arises from the similar local surface topology and surface chemical composition of the four proteins and that such local factors alone are sufficient to rationalize the hydration shell dynamics [20]. Within this framework, Cameron and colleagues have shown that in many hydrated proteins and cells and, in particular, in hydrated collagen the hydration compartments are the same, in number, size, and physical characteristics. These water compartments can be defined using their hydration fraction limits $h = \text{grams of water for 1 g of dry mass}$ [24–26]. Cameron and Fullerton concluded that the dynamics of water molecules in solution are affected even up to 10–11 Å from the protein surface and that the hydration water layer can be divided into 2–3 shells 3.5 Å thick. In addition, the results seem to give proof that within 6–7 Å reside water molecules in interaction with polar sites of the protein's surface, while between 7 Å and 9 Å, there are water molecules influenced by hydrophobic sites. Based on these results, they presented the molecular stoichiometric hydration model (SHM) which interprets the broadening of the hydration water dynamics in terms of a hydration monolayer up to $h = 1.6 \text{ g/g}$, divided into four water compartments with a well-fixed relative size. The dynamics of these molecules are slower than the bulk water that resides in the “compartment” defined by $h > 1.6 \text{ g/g}$. The SHM predicts and explains the commonly cited and measured “bound” water fraction of 0.2–0.4 g of water/g of dry mass on proteins and, in particular, in tendon/collagen type I [25, 26] to which an $h = 1.6 \text{ g/g}$, i.e., 1.6 g of water for 1 g of collagen correspond to a hydration layer thickness of 5.66 Å from the protein surface that is about two water layers. Cameron and colleagues demonstrate that the results of their experiments on model bovine collagen samples using different techniques converge with one another and with the results of different researchers on other proteins and cells and confirm the assignments of their hydration model [6]. The SHM model considers a monolayer with $h_m = 1.6 \text{ g/g}$ divided 50% into primary hydration with $h_{pr} = 0.8 \text{ g/g}$ on polar hydrophilic sites, and 50% into secondary hydration over hydrophobic surfaces $h_{se} = 0.8 \text{ g/g}$. In particular, the primary hydration water molecules hydrogen-bonded to collagen polar side chains have $h_{psc} = 0.54 \text{ g/g}$ with greater free energy and $h_{pmc} = 0.26 \text{ g/g}$ relative to the protein main chain hydration with the greater free energy binding which includes the Ramachandran water-bridge, with capacity $h_{Ra} = 0.0656 \text{ g/g}$. As proof of the validity of their model, they conducted measurements on proteins with variable hydration, isotherm rehydration from the vapor phase, NMR

(nuclear magnetic resonance) water titration, NMR freezing point depression, high G-force dehydration, and hydration force (osmotic compression) and, in particular, confirmed the SHM model for the type I collagen [26]. In addition, they showed that many other techniques confirmed their results, such as X-ray scattering, neutron scattering, dielectric spectroscopy, and NMR [7].

Collagen is the most abundant protein in mammals, making up about 25% to 35% of the whole-body protein content, whose 90% is type I. For these characteristics, collagen is central in our study. There are nearly 28 types of collagens, but collagen type I is the most common in skin, cornea, artery walls, bone, teeth, tendon, ligaments, vascular ligature, and organs [30, 49, 77, 80, 84].

Dielectric spectroscopy experiments

Dielectric spectroscopy can be used to obtain information on the dynamics of proteins. Among the many techniques, dielectric spectroscopy has the advantage to investigate the arrangement of water in confined systems, more generally in interfacial or restricted environments, over a wide time scale, providing information on the orientational dynamics of molecular dipoles and covering all kinds of polarization fluctuations in the milli- to picosecond time scales [9, 23]. Usually, the dielectric spectrum in protein solutions displays three main features, denoted as β , γ , and δ dispersion, which represent dielectric relaxation processes at well-separated timescales. In the past decades, many researchers have focused their efforts on this field. These studies provided useful information on the physicochemical properties of hydrated biomolecules and showed their dielectric spectrum from 1 MHz to tens of GHz. The early dielectric spectroscopy experiments conducted by Harvey and Hoekstra [39] on hydrated powders of lysozyme revealed two distinct dispersions with a relaxation time of near 1 ns (100–200 MHz) and near 0.02 ns (7–8 GHz), respectively [39]. This dispersion is related to the hydration water that Grant named δ -relaxation [32]. Many computer simulations and experiments with different techniques have been conducted so far to explain the rationale of the δ -dispersion [5, 9, 10, 18, 21, 33–35, 38, 46, 62, 64–66, 68, 72, 85]. The molecular dynamics (MD) simulations performed by Oleinikova, Cametti, Wolf, and, Steinhauser's group were particularly interesting [1, 9, 68, 89]. However, so far, no consensus on the physical origins of the δ -dispersions has yet been found.

We have focused on the works produced by Grant, Oleinikova, Cametti, and Wolf [9, 33, 34, 68, 89] that report on dielectric spectroscopy measurements and molecular dynamics simulations of protein in an aqueous solution at different concentrations and controlled conditions to characterize the δ -dispersion main features. Grant studied globular proteins in water solutions and, in particular, with Takashima measured the dielectric dispersion of Bovine Serum Albumin solutions (BSA molecular weight is 66.46 kDa at pH = 5.07 and $T = 293.15$ K), from MHz to GHz and concentrations from 724 to 1083 mg/mL (10.9–16.3 mM or $h = 0.64$ – 0.18), and collected results at different temperature and pH. They, using the mixture theory, have quantified the bound water fraction related to the δ -dispersion and verified that the bound water static permittivity ϵ_{SB} ranges from 100 to 300 depending on the concentration [33].

Oleinikova research group has used dielectric spectroscopy to study the dynamics of ribonuclease A in aqueous solutions (RNase A molecular weight 13.7 kDa at pH 5.5 and T

= 298.15 K) and concentration from 0.36 to 4.48 mM (or from 0 to 59.96 mg/mL or $h = 0.005\text{--}0.06$) [68]. They have decoded the complexity of the dielectric spectrum, comparing it to other experiments such as NMR techniques and molecular dynamics simulation of the autocorrelation function $\Phi(t)$ of the total collective dipole moment of the sample.

In particular, they decomposed $\Phi(t)$ in three self-components $\Phi_{pp}(t)$, $\Phi_{HH}(t)$, and $\Phi_{BB}(t)$ and three cross-correlation components $\Phi_{pH}(t)$, $\Phi_{pB}(t)$, and $\Phi_{HB}(t)$. The $\Phi_{pp}(t)$ was assigned to the β -dispersion due to the protein tumbling, with $\tau_{relax} = 20$ ns and $f_{relax} = 1$ MHz, the $\Phi_{BB}(t)$ to the γ -dispersion due to the bulk water reorientation. They confirmed the existence of three different states of hydration water. The $\Phi_{HH}(t)$ is related to the δ_3 dispersion, with $\tau_{relax} = 35$ ps and $f_{relax} = 4.55$ GHz, due to hydration water orientation polarization. Specifically, $\Phi_{pp}(t)$ is related to the δ_2 dispersion, with $\tau_{relax} = 500$ ps and $f_{relax} = 318.5$ MHz, concerning polar side chain fluctuation and, finally, the δ_1 dispersion, with $\tau_{relax} = 2$ ns and $f_{relax} = 79.6$ MHz, to protein water cross-correlation $\Phi_{pH}(t)$, which occurs near the β -protein relaxation. The δ_1 assignment was supported by MD simulation. In this picture, the cross-correlation between water and protein plays a major role confirmed later by Steinhäuser's group [5]. Cametti obtained the dielectric spectra of Lysozyme in aqueous solutions (lysozyme molecular weight is 14.3 kDa and partial specific volume is 0.73 mL/mg at pH = 5.5 and $T = 293.15$ K) and concentration from 1 to 125 mg/mL (0.1–8.7 mM that corresponds to a hydration $h > 7.26$) in the range of 1 MHz–50 GHz [9]. Wolf and his team studied the dynamics of aqueous lysozyme solutions in the frequency range from 1 MHz to 40 GHz in relation to concentration and temperatures ranging from 275 to 330 K, providing data on the temperature dependences of the β , δ , and γ -relaxations [89].

Methods

Given the negligible size of the cells making up the tissue, compared to the frequency range taken into consideration the electromagnetic homogenization theory can be applied [22, 50, 51, 53, 82]. We have used the Maxwell Garnett mixing formulae to perform the simulations and evaluate the tissue's permittivity and conductivity [49, 54, 90] and compare our different models. The effective permittivity of a material made by different constituents, such as protein solution or biological tissue, can be derived as a function of the constituent's fractional volumes and their permittivity at the frequency of interest [58, 59, 82]. For the binary system, we have used the Maxwell Garnett Eq. (1):

$$\epsilon_{eff}^*(f) = \epsilon_{host}^*(f) + 3\phi\epsilon_{host}^* \frac{\epsilon_i^*(f) - \epsilon_{host}^*(f)}{\epsilon_i(f) + 2\epsilon_{host}^*(f) - \phi[\epsilon_i^*(f) - \epsilon_{host}^*(f)]} \quad (1)$$

$\epsilon_i(f)$ and $\epsilon_{host}^*(f)$ are the complex permittivity of the inclusions and the host material at the same frequency f , while ϕ is the fractional volume of the inclusion. For a multiphase system made of N types of inclusions, we use Eq. (2) [58, 59, 82]:

$$\epsilon_{eff}^*(f) = \epsilon_{host}^*(f) + 3\epsilon_{host}^*(f) \frac{\sum_{n=1}^N \phi_n \frac{\epsilon_{i,n}^*(f) - \epsilon_{host}^*(f)}{\epsilon_{i,n}^*(f) + 2\epsilon_{host}^*(f)}}{1 - \sum_{n=1}^N \phi_n \frac{\epsilon_{i,n}^*(f) - \epsilon_{host}^*(f)}{\epsilon_{i,n}^*(f) + 2\epsilon_{host}^*(f)}} \quad (2)$$

To use the Maxwell Garnett formulas, we need to know the volume fraction and the Debye parameters of all the elements of our tissue models. We have computed the

permittivity and conductivity of a generic inclusion—hydration water compartment protein and lipid contents—using the Debye formula Eq. (3). The Debye formula Eq. (3) models the complex relative permittivity of fluids and other materials ε^* as a function of the frequency f , [13]. Equations (4) and (5) show the real and the imaginary parts of relative permittivity:

$$\varepsilon^*(f) = \varepsilon'(f) - j\varepsilon''(f) = \varepsilon_\infty + \frac{\varepsilon_s - \varepsilon_\infty}{1 + j\omega\tau} \quad (3)$$

$$\varepsilon'(f) = \varepsilon_\infty + \frac{\varepsilon_s - \varepsilon_\infty}{1 + \omega^2\tau^2} = \varepsilon_\infty + \frac{\varepsilon_s - \varepsilon_\infty}{1 + (f/f_r)^2} \quad (4)$$

$$\varepsilon''(f) = \frac{(\varepsilon_s - \varepsilon_\infty)\omega\tau}{1 + \omega^2\tau^2} = \frac{\sigma_d(f) + \sigma_s}{\varepsilon_0 2\pi f} \quad (5)$$

In Eqs. (3)–(5), $\omega = 2\pi f$ is the pulsation of the external field, τ is the relaxation time of the generic dipole of the system, ε_s is the static permittivity of the material and ε_∞ is its permittivity at field frequencies for $\omega\tau \gg 1$, $\sigma_d(f)$ is the frequency-dependent conductivity arising from dielectric polarization, while σ_s is the steady-state conductivity. The quantity $\varepsilon_s - \varepsilon_\infty$ is the change in the permittivity from very low frequencies to very high frequencies, compared to the relaxation frequency $f_r = \frac{1}{2\pi\tau}$.

The tissue models

In our procedure, the water in the hydration shell is divided into the four compartments (see Table 1) defined by the hydration SHM model in Fig. 1, proposed by Cameron and Fullerton [6–8]. In Table 1, there are the protein hydration limits and the four hydration compartment intervals h_i defined by the SHM used to compute the size of any compartments $D h_i$ in the protein hydration layer declared in Fig. 1.

Native tendon hydration has monolayer coverage on collagen $hm = 1.6$ g/g which divides into primary hydration on polar surfaces $hpp = 0.8$ g/g and secondary hydration $hs = 0.8$ g/g bridging over hydrophobic surfaces.

We introduced four hydration models based on homogenization theory to represent a generic human tissue as a mixture of hydrated proteins and adipocytes in a host of free water. The four hydration models, shown in Fig. 2, were then compared to one another. The hydration compartments in the protein hydration layer have been distributed into one to four shells. A generic protein with water in the hydration shell is constituted of four compartments defined by the hydration SHM model proposed by Cameron and Fullerton [6–8]. We have arbitrarily named these water species as super

Table 1 Protein hydration limits and the four hydration compartment intervals h_i defined by the SHM used to compute the size of any compartments in the protein hydration layer declared in Fig. 1

Protein hydration compartment	Min val.	Max val.	Δh_i
h1	0.000	0.066	0.066
h2	0.066	0.540	0.474
h3	0.540	0.800	0.260
h4	0.800	1.600	0.800

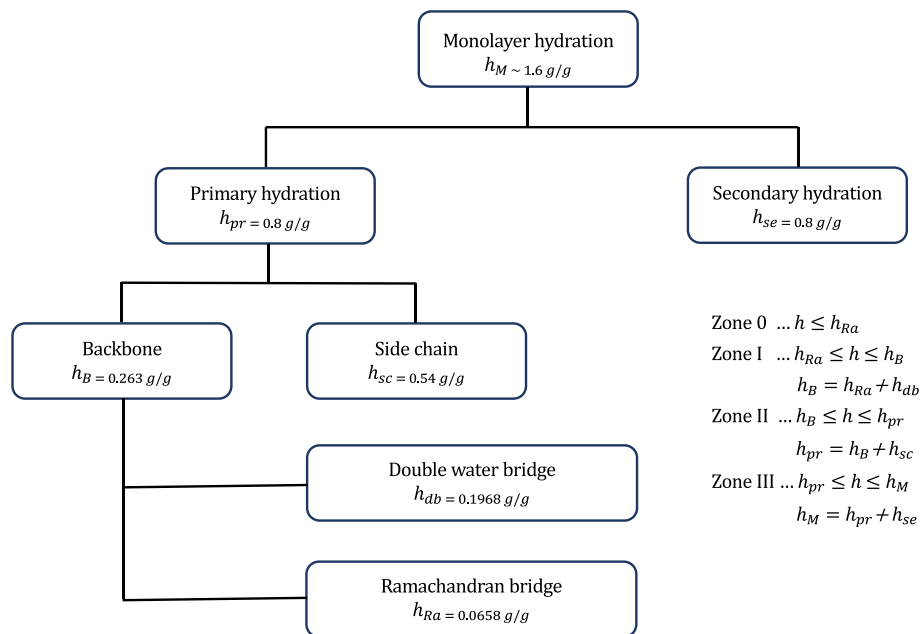


Fig. 1 Scheme of the Cameron and Fullerton SHM hydration model

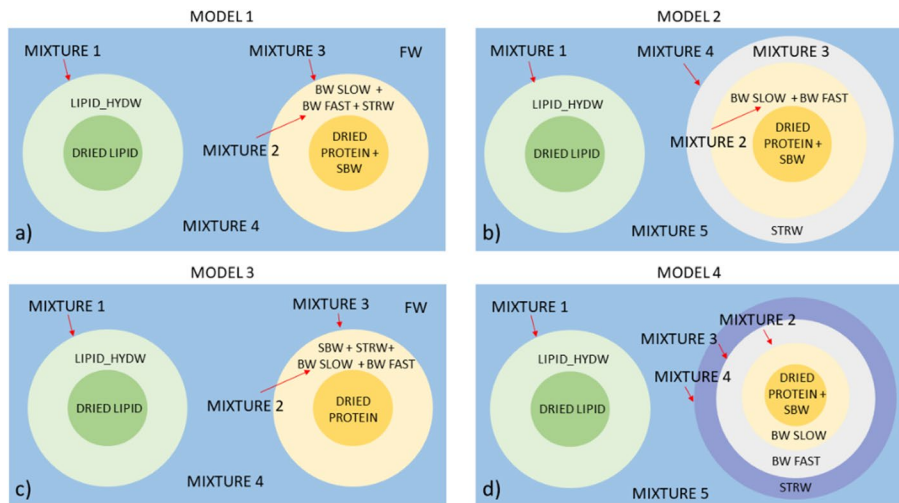


Fig. 2 a–d Depiction of the models 1–4 to homogenize the tissues. These are not in scale: hydrated protein size is 1–300 nm. We model an adipocyte, with a size around 20–300 μm, composed of a water coated fat globule with an outer radius $a = 100 \mu\text{m}$ and an inner radius $b = 80 \mu\text{m}$

bound water (SBW), bound water slow (BWS), bound water fast (BWF), and structured water (STRW). The size of any compartment of the “system” was then computed with the hydration intervals computed using the hydration limits of the SHM model, assuming for water, protein, and lipids a mass density equal to 0.997 g/ml, 1.39 g/ml, and 0.905 g/ml, respectively [56, 76]. Moreover, 1.10 g/ml was assumed for water over strongly hydrophilic solute and 0.85–0.90 g/ml for water over strongly hydrophobic solute [16, 19]. For a generic adipocyte fat cell, the model introduced in Said’s work was adopted [76]. The fat globules are water-coated and have an outer radius of $a = 100 \mu\text{m}$ and an

inner radius of $b = 80 \mu\text{m}$. We have imposed a hydration fraction $h = 0.278 \text{ g}$ of which 70% is structured water and 30% free water.

All proposed models are characterized by mixture 1 in common. Mixture 1 is a core-shell system. Dry lipid and hydrated lipid are present in the core and shell layer, respectively. In model 1 (see Fig. 2a), the protein system is a homogenized core-shell system. The core is a two-phase system: dry protein-SBW and a three-phase shell. The following three constituents: BW slow, BW fast, and STRW (mixture 2) are homogeneously distributed. In mixture 3, the Maxwell Garnett (MG) formula for a multi-phase system was used. Finally, a two-phase MG model was used between mixture 1 and mixture 2 to obtain the permittivity of model 1. In model 2 (see Fig. 2b), the protein system has three independent layers. Mixture 4 is composed of a two-phase system core with dry protein-SBW, a two-phase intermediate layer with BW slow and BW fast, and then an STRW layer. Each layer was modeled with the MG equation, including a top layer, obtaining mixtures 2, 3, and 4 each time. Finally, as in the previous case, the tissue was homogenized using the multi-phase MG equation. In model 3 (see Fig. 2c), as in the first model, the protein system has two independent layers (core-shell). The core consists of dry protein. The external layer is composed of BW slow, BW fast, SBW, and STRW (mixture 2). Mixture 2 is homogeneously distributed around the core. Mixture 3 was obtained using the MG model. Finally, the tissue's permittivity and conductivity were obtained with the homogenization of mixture 1, the hydrated lipid with mixture 3, and the hydrated protein. Model 4 presents the hydrated protein as a 4-layers system (see Fig. 2d). The core consists of a two-phase: SBW-dry protein. All the outer layers were considered monophasic and independent, in particular, from the innermost layer to the outermost one; there are BW slow, BW fast, and STRW, obtaining mixtures 1, 2, 3, and 4, respectively. As in all previous cases, the tissue homogenization has been computed using the MG model on mixture 1 and mixture 4. We modeled an adipocyte around 20–300 μm composed of a water-coated fat globule with an outer radius $a = 100 \mu\text{m}$ and an inner radius $b = 80 \mu\text{m}$.

The SBW compartment is related to the internal water molecules present in the protein cavities. For most purposes, internal water molecules are considered an integral part of the protein, even though they undergo the exchange mechanism with external water molecules, typically on a time scale of 0.1–10 μs [36, 37]. These molecules are added to our models to the protein compartment with the same Debye parameters. The BW water molecules are related to the δ -dispersion revealed by Haggis and Buchanan 10 years after Oncley's work showed the presence of β - and γ -relaxations in the late 1930s and 1940s. This dispersion is due to the dielectric relaxation of water near the protein surface. Detailed MD simulations interpret the broadening of this dispersion due to a faster contribution related to the protein-protein tern of the total electric dipole moment auto-correlation interaction and a slower one related to the component due to the protein-water interaction. Steinhauser's group, analyzing the collective nature of the dielectric experiment through the MD simulation, found three additional δ -terms related to the water-water self-correlation and a δ -term related to protein self-correlation in addition to the β - and γ -relaxations and the main δ -term due to the water protein cross-correlation [5]. Beyond the β - and γ -dispersions, we consider the two δ -dispersions related to protein-protein and water-proteins and the one near the γ -dispersion related to the

structured water influenced by hydrophobic interactions. We have named bound water slow the compartment related to δ_1 and bound water fast the compartment related to δ_2 ; these are computed as average of δ_1 and δ_2 [68].

The structured water compartment is indeed related to δ_3 ; we have computed about the γ -dispersion. With structured water, we intend the water molecules near hydrophobic sites. In the SHM hydration model, this compartment is related to the hydration interval $h = (0.8-1.6)$ g of water per g of solid. The water interacting with hydrophobic groups forms a “clathrate” structure. Computer simulations indicate that such modifications in water structure can extend at least 10 Å into the bulk liquid from the hydrophobic surface [71]. This compartment has a little slower dynamic than the bulk water [41, 67, 74]. Structured water molecules face hydrophobic sites and are a little slower than the free water molecules [11, 20, 31, 57, 63, 70]. We imposed the relaxation time of these water molecules to $\tau_{strw} = (1.4 - 2) \times \tau_{free\ water}$ [75].

Ultimately, the water molecules that are not affected by the presence of a solute are considered free. In our study, the Debye parameters for pure water at different temperatures were related to the data reviewed by Kaatz [42]. These data are shown in Table 2.

Debye parameters assignment

The SHM hydration model to reproduce the results of valuable studies on protein aqueous solution was first analyzed. We, then, considered these heterogeneous systems as a collection of spherical particles (the proteins) of complex dielectric constant $\epsilon_p^*(f)$ covered by a hydration shell composed of four water compartments with complex dielectric constant $\epsilon_{hi}^*(f)$, uniformly distributed in a continuous medium of free water with its own complex dielectric constant $\epsilon_m^*(f)$. In particular, the results of Oleinikova and co-workers were used [68], which studied the spectrum of RNase A in water at different concentrations and the spectrum of Lysozyme in aqueous solution reported by Cametti and colleagues both in the frequency range from 1 MHz to tens of GHz [9].

Then, we optimized the Debye parameters to reproduce the dielectric response of tendon/collagen in the frequency range 0.01–10 GHz. Finally, the complex permittivity of a generic human tissue assessing our results in comparison to the golden standard was estimated [29].

The size of the four compartments of our four mixture models, based on the hydration limits of the SHM model proposed by Cameron and Fullerton, was computed [6]. A generic hydrate system, protein aqueous solution, or human tissue, as a mixture of solid and water components, was modeled. The host is composed of free water;

Table 2 Debye parameters for pure water at different temperatures. These data were reviewed by Kaatz [42]

T (°C)	ϵ_s	ϵ_∞	τ (ps)
20	80.2 ± 0.2	5.6 ± 0.2	9.36 ± 0.05
25	78.36 ± 0.05	5.2 ± 0.1	8.27 ± 0.02
37	74.1 ± 0.2	4.6 ± 0.3	6.20 ± 0.05

the inclusions are the hydrated proteins and lipids and the hydration water compartments. The mixture's complex permittivity is computed using the MG mixture formulas. The volume fraction and the complex permittivity of any components of the mixture are the input of the model. The complex permittivity was computed with the Debye formula for each component ranging from 0.01 to 10 GHz assigning the Debye parameters: ε_s , ε_∞ , σ_i , and, τ_{relax} .

The aim was to reproduce the Oleinikova results about the dielectric spectrum of RNase A in an aqueous solution at concentrations of 4.34 mM, 298.15 K, and pH 5.5. We have imposed the relaxation times of any compartments using the Oleinikova results related to the dispersions β , γ , and the three δ_1 , δ_2 , and δ_3 . Then, the static permittivity ε_s and ε_∞ of any compartment were observed and optimized to reproduce the Oleinikova results.

Using the same parameters, we have, then, tested our procedure with the four protein hydration models shown in Fig. 2, reproducing the results of Cametti on lysozyme aqueous solutions. In these cases, we have scaled the ε_s considering for RNase A $\mu_0 = 280$ D and $MW = 13690$ Da, while for lysozyme $\mu_0 = 210$ D and $MW = 14300$ Da. For this purpose, Onsager-Onsager's model relation, which connects the proportionality between the $\Delta\beta$ increment and the effective dipole moment volume density of the protein solution, was used [72, 78]:

$$\Delta\varepsilon' = N_A c g_k \mu_0^2 / (2\varepsilon_0 MW k T) \quad (6)$$

where N_A is Avogadro's number, k is the Boltzmann constant, c is the concentration in kg/m^3 of the polar molecule in the solvent, and g_k is a parameter introduced by Kirkwood [44, 45] to account for molecular associations and correlation effects between the motions of solute and solvent molecules. The μ_0 is the dipole moment of an isolated molecule, $g_k \mu_0^2 = \mu_{\text{eff}}^2$ is the effective squared dipole moment per molecule in the ensemble, C (mM) = $c(\text{mg/ml})/MW(\text{g/mole})$ is the concentration expressed in millimoles per liter, while $N_A C$ (mM) is the protein/dipole volume density.

Next, using again the SHM hydration model, we have optimized the free parameters of our models to best attain the dielectric spectrum of the tendon/collagen. The tendon in human tissue is composed on average of 61.54% water, 37.46% proteins and other solid not lipids, and 1% lipids. This average composition corresponds to a "concentration" of 420 mg/mL. We used Onsager-Onsager's model to correct the $\Delta\beta$ computed to reproduce the RNase A dispersion and the scale factor to compute the ε_s for the protein considered in the simulation. In the case of collagen type I with $\mu_0 = 15000$ D and molecular weight (MW) = 324000 Da, considering for RNase A $\mu_0 = 280$ D and molecular weight (MW) = 13700 Da, the following was obtained:

$$\mu_0^2/MW [\text{collagen, type I}]/\mu_0^2/MW [\text{RNaseA}] = 722.614/5.515 = 131.$$

For more details on the methods, refer to the "Supporting information" document.

Debye parameters assignation for RNase A and human tissues

In Tables 3 and 4, there are the Debye parameters optimized to reproduce the dielectric spectrum of 4.34 mM RNase A aqueous solution and tendon tissue in which

Table 3 Debye parameters chosen to reproduce the RNase A aqueous solution at 4.38 mM concentration

DEBYE PARAMETERS	POOL 1 HYDRATED PROTEIN	POOL 2 HYDRATED LIPID	POOL 3 SBW	POOL 4 LIPID STRW	POOL 5 BW SLOW	POOL 6 BW FAST	POOL 7 STRW	POOL 8 FW
τ_{min} (s)	2.394E-08	1.590E-08	2.394E-08	1.590E-08	1.558E-09	3.306E-11	1.158E-11	8.270E-12
τ_{max} (s)	2.646E-08	1.590E-08	2.646E-08	1.590E-08	1.722E-09	3.654E-11	1.158E-11	8.270E-12
ϵ_{smin}	400.000	2.500	400.000	10.000	180.000	180.000	109.704	78.360
ϵ_{smax}	400.000	2.500	400.000	30.000	180.000	180.000	109.704	78.360
ϵ_{∞_min}	5.200	2.200	5.200	5.200	5.200	5.200	5.200	5.200
ϵ_{∞_max}	5.200	2.200	5.200	5.200	5.200	5.200	5.200	5.200
σ_{L_min} (S/m)	0.300	3.000E-07	0.300	0.300	0.300	0.300	0.300	0.300
σ_{L_max} (S/m)	0.300	7.000E-07	0.300	0.300	0.300	0.300	0.300	0.300
f_{min} (Hz)	5.000E+08	5.000E+08	5.000E+08	5.000E+08	5.000E+08	5.000E+08	5.000E+08	5.000E+08
f_{max} (Hz)	1.000E+10	1.000E+10	1.000E+10	1.000E+10	1.000E+10	1.000E+10	1.000E+10	1.000E+10
f_{min} (Hz) relax	6.015E+06	4.974E+04	6.015E+06	4.974E+04	9.242E+07	4.356E+09	1.375E+10	1.924E+10
f_{max} (Hz) relax	6.648E+06	1.001E+06	6.648E+06	1.001E+06	1.022E+08	4.814E+09	1.375E+10	1.924E+10

Table 4 Debye parameters optimized for tendon/collagen type I about the average tissue composition reviewed by Duck [17] and regarding the average dielectric tendon characteristics collected by Gabriel and co-workers [29], our golden standard. We propose to use these parameters to reproduce the complex permittivity (ϵ' and σ) of a generic human tissue based on its water and solid content (see Supporting information, Eq. (S2))

DEBYE PARAMETERS	POOL 1 HYDRATED PROTEIN	POOL 2 HYDRATED LIPID	POOL 3 SBW	POOL 4 LIPID STRW	POOL 5 BW SLOW	POOL 6 BW FAST	POOL 7 STRW	POOL 8 FW
τ_{min} (s)	6.840E-07	1.590E-08	6.840E-07	1.590E-08	6.134E-09	2.607E-11	1.179E-11	6.200E-12
τ_{max} (s)	7.560E-07	1.590E-08	7.560E-07	1.590E-08	6.606E-09	2.807E-11	1.269E-11	6.200E-12
ϵ_{smin}	50497.558	2.500	50497.558	180.000	180.000	180.000	103.740	74.100
ϵ_{smax}	50497.558	2.500	50497.558	180.000	180.000	180.000	103.740	74.100
ϵ_{∞_min}	2.500	2.500	2.500	2.500	2.500	2.500	2.500	2.500
ϵ_{∞_max}	5.200	2.500	5.200	2.500	5.200	5.200	5.200	5.200
σ_{L_min} (S/m)	0.250	3.500E-02	0.250	0.035	0.250	0.250	0.250	0.250
σ_{L_max} (S/m)	0.250	3.500E-02	0.250	0.035	0.250	0.250	0.250	0.250
f_{min} (Hz)	5.000E+08	5.000E+08	5.000E+08	5.000E+08	5.000E+08	5.000E+08	5.000E+08	5.000E+08
f_{max} (Hz)	1.000E+10	1.000E+10	1.000E+10	1.000E+10	1.000E+10	1.000E+10	1.000E+10	1.000E+10
f_{min} (Hz) relax	2.105E+05	1.001E+07	2.105E+05	1.001E+07	2.409E+07	5.670E+09	1.254E+10	2.567E+10
f_{max} (Hz) relax	2.327E+05	1.001E+07	2.327E+05	1.001E+07	2.595E+07	6.105E+09	1.350E+10	2.567E+10

100 g are, on average, divided as follows: 61.54 g of water, 1 g of lipids, and 37.46 g of collagen type I that correspond to a concentration of 245.20 mg/mL or 1.47 mM. In particular, for tendon/collagen type I, RNase A, and lysozyme, we have found $\epsilon_{SB} \approx 100-180$ in line with the values found by Grant [33, 34].

Results

The current procedure and models were assessed through simulations using a home-made MatLab script. As previously mentioned, all the models are based on MG formulas. In the cases where more than two spheres were considered, the Transmission-Matrix technique and Morse–Feshbach formulas were implemented numerically [3, 14, 15, 50–52, 55].

The input of our simulations is the protein concentration for protein solutions obtained from the Oleinikova and Cametti works on RNase A and lysozyme aqueous solutions, while the tissue's content in terms of water, lipid, and solid fractions are obtained from the Duck review [17]. To correct the Debye parameters for using the protein solutions at 20 °C, the values were rescaled at 37 °C for human tissues [89] (for more information, refer to [Supporting information materials](#)). In Fig. 3, the simulations for the protein aqueous solutions made with model 3 are shown. In Fig. 4, the simulations for tendon, on the left, and adipose tissues, on the right, made with model 3 are also shown. We use these simulations to validate our procedure and modelization of protein hydrated systems. We compare the deviation from the experimental traces published independently by Oleinikova for RNase A aqueous solutions, Cametti for lysozyme aqueous solutions, and the traces published by Gabriel for human tissues (their results are the golden standard we consider in these simulations). We have computed the root mean square relative error percentage (RMSRE%) in order to assess the results of our simulations performed using a homemade MatLab script. In our simulation, the deviation for the permittivity is less than 10%, while for the conductivity, the errors % of our results compared to the experimental are around 20–30% in the frequency range 0.01–10 GHz.

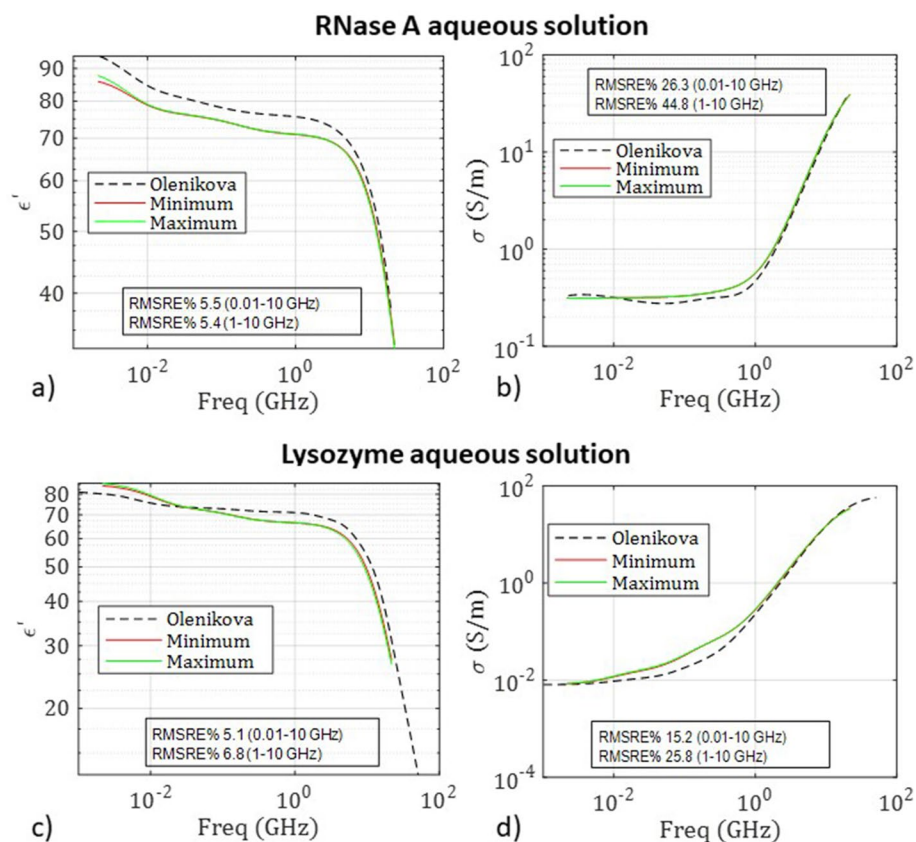


Fig. 3 RNase A 4.38 mM aqueous solution (on top) and 7.69 mM lysozyme aqueous solution (on bottom) results of simulation made with model 3. The golden standards are from Oleinikova and Cametti data [9, 68]

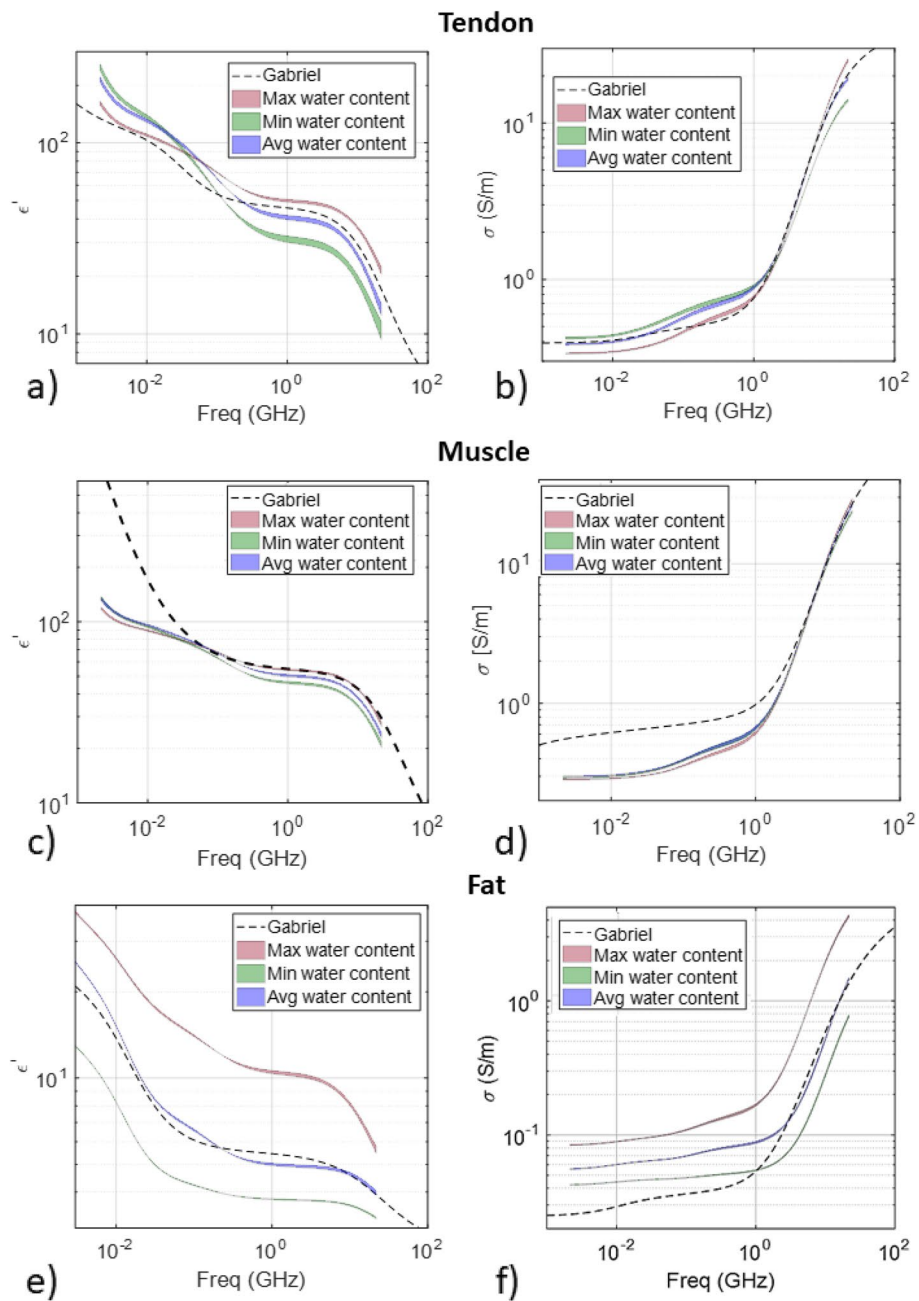


Fig. 4 From the top simulation results for the human tendon (**a** and **b**), human muscle (**c** and **d**), and adipose tissue (**e** and **f**). In the left column, the imaginary part of the complex dielectric permittivities is represented, and on the right column, the conductivity is represented

The assessment of our models 1–4 were conducted with simulations using MG formulation and computing the root mean squared relative error % (RMSRE%) in Eq. (6) compared to the golden standard.

$$RMSRE\% = 100 \sqrt{\frac{1}{N} \sum_{i=1}^N \frac{[x^m - x^{GS}]^2}{x^{GS}}} \tag{6}$$

Tables 5 and 6 show the RMSRE% for ϵ' and σ evaluated with the simulations, using the 4 homogenization models, in two different frequency ranges 0.01–10 GHz and 1–10 GHz for a 4.34 mM RNase A and a 7.79 mM lysozyme aqueous solution. From these tables, it can be seen that for both protein solutions, model 3 is the one that provides a lower RMSRE%, i.e., the model with all water species (SBW, BWS, BWF, and STRW) homogenized in a single layer around the dry protein

In Table 7 is model 1–4 assessment for human tissue tendon, muscle, and fat, while the results for seven selected human tissues are shown in Table 8. The golden standards are data from Oleinikova's and Cametti's experimental results on the protein solutions [9, 68] and Gabriel's experimental data on human tissues [29]. Simulation results are shown; model 3 gives the best results for both protein solutions and most human tissues simulations.

In this work, we are interested to the dielectric relaxation processes at lower microwaves occurring from 1 GHz to 10 GHz, where the dipolar relaxation of tissue water occurs and from 0.1 to 4.5 GHz from dielectric relaxation of the “bound” water near the protein surface, and the protein polar sidechains. We have used the Onsager-Onccley's equation to improve our model connecting the lower limit of our band of interest (0.1-10 GHz) to the β -dispersion (1 kHz to several MHz).

In this way, we have considered the $\Delta\epsilon'$ increment associated with the polarization of proteins and other organic macromolecules. In reality the β -dispersion is the result of more mechanisms, for example the ionic conductivity of cell membranes that our model does not control. This is the reason of the high deviation for ϵ' of muscle from the Gold Standard at low frequencies.

Conclusions

The aim was to prove the feasibility of realizing an automatic non-invasive methodology to estimate the dielectric properties in vivo of a generic human tissue and to create both a permittivity and a conductivity map in the microwave frequency range from 1 to 10 GHz. We propose a heuristic method as a base to realize an automatic and non-invasive procedure to obtain an ad hoc dielectric mapping of human tissues in vivo, with a standard magnetic resonance imaging (MRI) scanner for medical imaging to quantify the water (free and bound), the lipid content, and the bone content. The homogenization theory was adopted in the study because, in the considered frequency range, the protein sizes were always much shorter than $\lambda_{\min} \sim 5 \times 10^{-3}$ m.

This method can be, particularly, useful in medical applications where the exact knowledge of the patient's anatomy and related electromagnetic properties would be of great benefit for the success of the treatment. Collagen type I is considered the prototype of the human tissue proteins in our models. First, the evaluation of the complex permittivity of a 4.34 mM RNase A aqueous solution at room temperature was performed to fix the Debye parameters. Our methodology was validated by evaluating the dielectric spectrum of a 7.69 mM lysozyme aqueous solution and the permittivity and conductivity of tendon/collagen human tissue in the frequency range from 0.01 to 10 GHz.

Then, using the collagen/tendon-optimized Debye parameters and MG mixture formulas, we evaluate the complex permittivity of human tissues. Comparing our results to

Table 5 RNase A (4.38 mM aqueous solution) model 1-4 simulations. Average RMSRE% for ϵ' and σ on the ranges 0.01-10 GHz and 1-10 GHz (in green is highlighted the best average RMSRE%)

RNase A Model 1				RNase A Model 2			
0.01-10 GHz		1-10 GHz		0.01-10 GHz		1-10 GHz	
RMSRE% ϵ'	RMSRE% σ	RMSRE% ϵ'	RMSRE% σ	RMSRE% ϵ'	RMSRE% σ	RMSRE% ϵ'	RMSRE% σ
5.2	15.4	6.8	26.0	45.9	156.4	57.3	267.1
AVG RMSRE%		AVG RMSRE%		AVG RMSRE%		AVG RMSRE%	
12.9		19.9		124.0		190.9	
RNase A Model 3				RNase A Model 4			
0.01-10 GHz		1-10 GHz		0.01-10 GHz		1-10 GHz	
RMSRE% ϵ'	RMSRE% σ	RMSRE% ϵ'	RMSRE% σ	RMSRE% ϵ'	RMSRE% σ	RMSRE% ϵ'	RMSRE% σ
5.2	15.2	6.8	25.8	4.9	18.9	6.5	32.2
AVG RMSRE%		AVG RMSRE%		AVG RMSRE%		AVG RMSRE%	
12.8		19.7		14.4		22.6	

Table 6 Lysozyme (7.68 mM aqueous solution) model 1–4 simulations. Average RMSRE% for ϵ' and σ on the ranges 0.01–10 GHz and 1–10 GHz. ϵ_s (protein) rescaled for $[\mu^2/\text{MW} (\text{Lysozyme})/\mu^2/\text{MW} (\text{RNaseA})]$

Lysozyme Model 1			Lysozyme Model 2		
0.01-10 GHz		1-10 GHz	0.01-10 GHz		1-10 GHz
RMSRE% ϵ'	RMSRE% σ	RMSRE% ϵ'	RMSRE% σ	RMSRE% ϵ'	RMSRE% σ
5.5	26.4	5.4	44.9	47.7	112.1
AVG RMSRE%		AVG RMSRE%		AVG RMSRE%	
18.8		27.9		103.8	
Lysozyme Model 3			Lysozyme Model 4		
0.01-10 GHz		1-10 GHz	0.01-10 GHz		1-10 GHz
RMSRE% ϵ'	RMSRE% σ	RMSRE% ϵ'	RMSRE% σ	RMSRE% ϵ'	RMSRE% σ
5.4	26.4	5.4	44.8	5.4	28.3
AVG RMSRE%		AVG RMSRE%		AVG RMSRE%	
18.6		27.8		19.6	
				29.3	

Table 7 Selected human tissues (tendon, muscle, and fat) simulation results. RMSRE% for both ϵ' and σ of model 3 for ϵ_s (protein) rescaled for [μ^2 /MW (collagen type I)]/ μ^2 /MW (RNaseA)] on the range 0.01–10 GHz and 1–10 GHz

Tissue	RMSRE (%) ϵ'		RMSRE (%) σ'	
	0.01–10 (GHz)	1–10 (GHz)	0.01–10 (GHz)	1–10 (GHz)
Model 1				
Fat	6.4	5.7	77.7	27.5
Muscle	13.3	7.6	37.1	18
Tendon	19.1	10	14.4	6.6
Avg (RMSRE (%) ϵ' , σ)	0.01–10 (GHz)	1–10 (GHz)		
Fat	42.05	16.6		
Muscle	25.2	12.8		
Tendon	16.75	8.3		
Avg tissues	28	12.56		
Model 2				
Fat	> 100	> 100	> 100	> 100
Muscle	19	26.7	18.9	10.2
Tendon	20.1	6.6	16.4	11.6
Avg (RMSRE (%) ϵ' , σ)	0.01–10 (GHz)	1–10 (GHz)		
Fat	> 100	> 100		
Muscle	18.95	18.45		
Tendon	18.25	9.1		
Avg tissues	45.7333	42.51		
Model 3				
Fat	6.5	5.7	3.6	3.9
Muscle	13.5	7.7	37.1	17.9
Tendon	18.9	10.3	9	5.8
Avg (RMSRE (%) ϵ' , σ)	0.01–10 (GHz)	1–10 (GHz)		
Fat	5.05	4.8		
Muscle	25.3	12.8		
Tendon	13.95	8.05		
Avg tissues	14.76	8.55		
Model 4				
Fat	6.4	5.7	77.7	27.5
Muscle	12.6	4.6	38.4	17.2
Tendon	16.7	4.9	12.9	16.7
Avg (RMSRE (%) ϵ' , σ)	0.01–10 (GHz)	1–10 (GHz)		
Fat	42.05	16.6		
Muscle	25.5	10.9		
Tendon	14.8	10.8		
Avg tissues	27.45	12.76		

a golden standard, it was found that the estimated permittivity and conductivity showed a 13.2% RMSRE% on average.

Since we have used data relative to the average human tissue composition and average human tissue permittivity and conductivity from two different databases, we believe that these promising preliminary results lead to the next phase of this research.

The next step of this research will consist of involving animal ex vivo samples. The aim will be, first of all, to quantify the real sample composition in terms of water and

Table 8 Seven selected human tissues model 1–4 simulations. Average RMSRE% for ϵ' and σ of on the ranges 0.01–10 GHz and 1–10 GHz. ϵ_s (protein) rescaled for $[\mu^2/\text{MW} (\text{Collagen})/\mu^2/\text{MW} (\text{RNaseA})]$

Tissue	RMSRE (%) ϵ'		RMSRE (%) σ'	
	0.01–10 (GHz)	1–10 (GHz)	0.01–10 (GHz)	1–10 (GHz)
Model 1				
Cartilage	21.3	24.3	8.4	10.9
Eye corneal	19.7	3.7	50.4	29.7
Fat	6.4	5.7	77.7	27.5
Liver	21.9	15.8	19.1	17.3
Muscle	13.3	7.6	37.1	18
Skin	30.6	4.7	38.5	63.4
Tendon	19.1	10	14.4	6.6
Avg (RMSRE (%) ϵ', σ)	0.01–10 (GHz)	1–10 (GHz)		
Cartilage	14.85	17.6		
Eye corneal	35.05	16.7		
Fat	42.05	16.6		
Liver	20.5	16.55		
Muscle	25.2	12.8		
Skin	34.55	34.05		
Tendon	16.75	8.3		
Avg tissues	26.9929	17.5143		
Model 2				
Cartilage	12.3	5.4	16.6	13.4
Eye corneal	23.3	24.5	38.9	19.7
Fat	100	100	100	100
Liver	13.1	9.7	17.1	15.9
Muscle	19	26.7	18.9	10.2
Skin	22.9	8.4	91.5	100
Tendon	20.1	6.6	16.4	11.6
Avg (RMSRE (%) ϵ', σ)	0.01–10 (GHz)	1–10 (GHz)		
Cartilage	14.45	9.4		
Eye corneal	31.1	22.1		
Fat	100	100		
Liver	15.1	12.8		
Muscle	18.95	18.45		
Skin	57.2	54.2		
Tendon	18.25	9.1		
Avg tissues	36.4357	32.2929		
Model 3				
Cartilage	21.3	24.1	8.3	10.6
Eye corneal	19.8	3.5	50.3	29.8
Fat	6.5	5.7	3.6	3.9
Liver	22	15.7	19	17.2
Muscle	13.5	7.7	37.1	17.9
Skin	23.7	6.6	32.3	25.6
Tendon	18.9	10.3	9	5.8
Avg (RMSRE (%) ϵ', σ)	0.01–10 (GHz)	1–10 (GHz)		
Cartilage	14.8	17.35		
Eye corneal	35.05	16.65		
Fat	5.05	4.8		
Liver	20.5	16.45		

Table 8 (continued)

Tissue	RMSRE (%) ϵ'		RMSRE (%) σ'	
	0.01–10 (GHz)	1–10 (GHz)	0.01–10 (GHz)	1–10 (GHz)
Muscle	25.3	12.8		
Skin	28	16.1		
Tendon	13.95	8.05		
Avg tissues	20.3786	13.1714		
Model 4				
Cartilage	24.6	31.2	12.3	20.5
Eye corneal	20.4	7.9	51	27.6
Fat	6.4	5.7	77.7	27.5
Liver	23.6	20.2	21.6	18.9
Muscle	12.6	4.6	38.4	17.2
Skin	25	12.6	39.6	46.7
Tendon	16.7	4.9	12.9	16.7
Avg (RMSRE (%) ϵ', σ)	0.01–10 (GHz)	1–10 (GHz)		
Cartilage	18.45	25.85		
Eye corneal	35.7	17.75		
Fat	42.05	16.6		
Liver	22.6	19.55		
Muscle	25.5	10.9		
Skin	32.3	29.65		
Tendon	14.8	10.8		
Avg tissues	27.3429	18.7286		

the solid fraction, and this will be achieved using specific quantitative magnetic resonant (qMRI) sequences [40, 81]. In addition, with these MRI sequences, we can measure the free and bound water fractions in the sample [40, 81]. Finally, we will try to implement an MRI procedure to estimate the pH of the sample [86, 87, 91]. In this way, we are confident to be able to better fix the static conductivity of the sample, s_p , that we have arbitrarily fixed at $\sigma_i = 0.250$ S/m in this first investigation, taking the value reported in the literature for living tendon tissue at $T = 37$ °C [29].

Abbreviations

BSA	Bovine serum albumin
BWF	Bound water fast
BWS	Bound water slow
HTP	Hyperthermia treatment planning
MD	Molecular dynamics
MG	Maxwell Garnett
MRI	Magnetic resonance imaging
MW	Molecular weight
NMR	Nuclear magnetic resonance
qMRI	Quantitative magnetic resonant imaging
RMSRE%	Root mean square relative error percentage
RNaseA	Ribonuclease A
SBW	Super bound water
SHM	Stoichiometric hydration model
STRW	Structured water

Supplementary Information

The online version contains supplementary material available at <https://doi.org/10.1186/s44147-023-00187-8>.

Additional file 1.

Acknowledgements

Not applicable.

Authors' contributions

The manuscript was written through contributions of all authors. All authors have given approval to the final version of the manuscript.

Funding

This study had no funding from any resource.

Availability of data and materials

The datasets generated during and/or analyzed during the current study are available from the corresponding author on reasonable request.

Declarations

Ethics approval and consent to participate

Not applicable.

Consent for publication

Not applicable.

Competing interests

The authors declare that they have no competing interests.

Received: 15 December 2022 Accepted: 17 February 2023

Published online: 12 May 2023

References

1. Boresch S et al (2000) "Studying the Dielectric Properties of a Protein Solution by Computer Simulation," *J Phys Chem B* 104:8743–8752
2. Batool S et al (2019) Benefits and hazards of electromagnetic waves, telecommunication, physical and biomedical: a review. *Eur Rev Med Pharmacol Sci* 23(7):3121–3128
3. Batool S et al (2022) Multiple scattering by two PEC spheres using translation addition theorem. *Electronics* 11(1):126–139
4. Bernardi P et al (1997) Assessment of the potential risk for humans exposed to millimeter-wave wireless LANs: the power absorbed in the eye. *Wirel Netw* 3:511517
5. Braun D et al (2017) Towards a complete characterization of the δ -dispersion in dielectric spectroscopy of protein-water systems. *Phys Chem Chem Phys* 19:26980–26985
6. Cameron IL et al (2007) Verification of simple hydration/dehydration methods to characterize multiple water compartments in tendon type 1 collagen. *Cell Biol Int* 31(6):531–539
7. Cameron IL et al (2011) The molecular stoichiometric hydration model (SHM) as applied to tendon/collagen, globular proteins and cells. *Cell Biol Int* 35(12):1205–1215
8. Cameron IL, Fullerton GD (2014) Properties and size of multiple non-bulk water fractions on proteins and in cells. *Water J* 6:76–90
9. Cametti C et al (2011) Dielectric relaxation spectroscopy of lysozyme aqueous solutions: analysis of the delta-dispersion and the contribution of the hydration water. *J Phys Chem* 115:7144–7153
10. Cerveny S et al (2008) Universal features of water dynamics in solutions of hydrophilic polymers, biopolymers, and small glass-forming materials. *Phys Rev E Stat Nonlinear Soft Matter Phys* 77(3 Pt 1):031803
11. Charkhesht A et al (2018) High-precision megahertz-to-terahertz dielectric spectroscopy of protein collective motions and hydration dynamics. *J Phys Chem B* 122(24):6341–6350
12. Christ A et al (2010) The Virtual Family—development of surface-based anatomical models of two adults and two children for dosimetric simulations. *Phys Med Biol* 55:N23–N38
13. Debye P (1929) *Polar molecules*. Dover New York
14. Dinia L et al (2020a) Electromagnetic scattering of inhomogeneous plane wave by ensemble of cylinders. *J Telecommun Inf Technol* 3:86–92
15. Dinia L et al (2020b) Electromagnetic scattering between an elliptically inhomogeneous plane wave and a multilayered cylinder. *J Electromagn Waves Appl* 34(18):2455–2466
16. Doshi DA et al (2005) Reduced water density at hydrophobic surfaces: effect of dissolved gases. *Proc Natl Acad Sci U S A* 102(27):9458–9462
17. Duck FA (1990) *Physical properties of tissue: a comprehensive reference book*. Bath Academic Press
18. Fenimore PW et al (2013) Concepts and problems in protein dynamics. *Chem Phys* 424:2–6
19. Fischer H et al (2004) Average protein density is a molecular-weight-dependent function. *Protein Sci* 13:2825–2828

20. Fogarty AC, Laage D (2014) Water dynamics in protein hydration shells: the molecular origins of the dynamical perturbation. *J Phys Chem B* 118(28):7715–7729
21. Frauenfelder H et al (2009) A unified model of protein dynamics. *Proc Natl Acad Sci U S A* 106(13):5129–5134
22. Frezza F, Mangini F (2015) Vectorial spherical-harmonics representation of an inhomogeneous elliptically polarized plane wave. *JOSA A* 32(7):1379–1383
23. Frezza F et al (2015) In silico validation procedure for cell volume fraction estimation through dielectric spectroscopy. *J Biol Phys* 41:223–234
24. Fullerton GD, Cameron IL (1986) An evaluation of the hydration of lysozyme by an NMR titration method. *Biochim Biophys Acta* 869(3):230–246
25. Fullerton GD et al (2006) An NMR method to characterize multiple water compartments on mammalian collagen. *Cell Biol Int* 30(1):66–73
26. Fullerton GD, Cameron IL (2007) Water compartments in cells. *Methods Enzymol* 428:128
27. Gabriel S et al (1996a) The dielectric properties of biological tissues: I. Literature survey. *Phys Med Biol* 41(11):2231–2249
28. Gabriel S et al (1996b) The dielectric properties of biological tissues: II. Measurements in the frequency range 10 Hz to 20 GHz. *Phys Med Biol* 41(11):2251–2269
29. Gabriel S et al (1996c) The dielectric properties of biological tissues: III. Parametric models for the dielectric spectrum of tissues. *Phys Med Biol* 41:2271–2293
30. Gelse K et al (2003) Collagens—structure, function, and biosynthesis. *Adv Drug Deliv Rev* 55:1531–1546
31. Ghosh R et al (2014) Sensitivity of polarization fluctuations to the nature of protein-water interactions: study of biological water in four different protein-water systems. *J Chem Phys* 141:22D531
32. Grant EH (1962) Electrical behaviour of egg albumen solutions at ultra-high frequencies. *Nature* 196:1194–1195
33. Grant EH et al (1968) The dielectric behavior of aqueous solutions of bovine serum. *J Phys Chem* 72:4373–4380
34. Grant EH et al (1978) Dielectric behavior of biological molecules in solution. Clarendon Press, Oxford University Press, Oxford and London
35. Grimaldo M et al (2019) Dynamics of proteins in solution. *Q Rev Biophys* 52(E7):1–63
36. Halle B (1998) Water in biological systems: the NMR picture. In: Bellissent-Funel M-C (ed) *Hydration processes in biology*. IOS Press, Dordrecht, pp 233–249
37. Halle B (2004) Protein hydration dynamics in solution: a critical survey. *Philos Trans R Soc B* 359:1207–1224
38. Hande VR, Chakrabarty S (2022) How far is “bulk water” from interfaces? Depends on the nature of the surface and what we measure. *J Phys Chem B* 126:1125–1135
39. Harvey S, Hoekstra P (1972) Dielectric relaxation spectra of water adsorbed on lysozyme. *J Phys Chem* 76(21):2987–2994
40. Henkelman RM et al (2001) Magnetization transfer in MRI: a review. *NMR Biomed* 14:57–64
41. Kaatzte U (1989) Complex permittivity of water as a function of frequency and temperature. *J Chem Eng Data* 34(4):371–374
42. Kaatzte U (1997) The dielectric properties of water in its different states of interaction. *J Solut Chem* 26:1049–1112
43. Kaatzte U (2011) Bound water: evidence from and implications for the dielectric properties of aqueous solutions. *J Mol Liq* 162:105–112
44. Kirkwood JG (1939) The dielectric polarization of polar liquids. *J Chem Phys* 7:911–919
45. Kirkwood JG, Shumaker JB (1952) The influence of dipole moment fluctuations on the dielectric increment of proteins in solution. *Proc Natl Acad Sci U S A* 38(10):855–862
46. Khodadadi S, Sokolov AP (2017) Atomistic details of protein dynamics and the role of hydration water. *Biochim Biophys Acta Gen Subj* 1861(1 Pt B):3546–3552
47. Kok HP et al (2015) Current state of the art of regional hyperthermia treatment planning: a review. *Radiat Oncol* 10(196):1–14
48. Laage D et al (2017) Water dynamics in the hydration shells of biomolecules. *Chem Rev* 117:10694–10725
49. López AL et al (2019) Hydrolyzed collagen—sources and applications. *Molecules* 24(22):4031–4046
50. Mangini F et al (2014a) Analysis of the polarizability of an array of spherical metallic inclusions in a dielectric host sphere. *JOSA A* 31(11):2409–2414
51. Mangini F et al (2014b) Electromagnetic interaction with two eccentric spheres. *JOSA A* 31(4):783–789
52. Mangini F et al (2014c) Homogenization of a multilayer sphere as a radial uniaxial sphere: features and limits. *J Electromagn Waves Appl* 28(8):916–931
53. Mangini F, Tedeschi N (2017) Scattering of an electromagnetic plane wave by a sphere embedded in a cylinder. *JOSA A* 34(5):760–769
54. Mangini F et al (2018) Numerical analysis of electromagnetic interactions by a cell during the mitosis phases. *Int J Numer Methods Biomed Eng* 34(9):e3110. <https://doi.org/10.1002/cnm.3110>
55. Mangini F et al (2019) Electromagnetic scattering by a cylinder in a lossy medium of an inhomogeneous elliptically polarized plane wave. *J Telecommun Inf Technol* 4:36–42
56. Martin AD et al (1994) Adipose tissue density, estimated adipose lipid fraction and whole body adiposity in male cadavers. *Int J Obes Relat Metab Disord* 18(2):79–83
57. Martini S, Bonechi C, Foletti A, Rossi C (2013) “Water-Protein Interactions: The Secret of Protein Dynamics”, *Sci World J* 2013(138916):6. <https://doi.org/10.1155/2013/138916>
58. Maxwell Garnett JC (1904) Colours in metal glasses and in metallic films. *Philos Trans R Soc Lond* 203:385–420
59. Maxwell Garnett JC (1906) Colours in metal glasses, in metallic films, and in metallic solutions II. *Philos Trans R Soc Lond* 205:237–288
60. Mazzurana M et al (2003) A semi-automatic method for developing an anthropomorphic numerical model of dielectric anatomy by MRI. *Phys Med Biol* 48:3157–3170
61. Mocchi P et al (2021) Steerable3D: an ImageJ plugin for neurovascular enhancement in 3-D segmentation. *Phys Med* 81:197–209

62. Miura N et al (1994) Microwave dielectric study on bound water of globule proteins in aqueous solution. *Biopolymers* 34(3):357–364
63. Mukherjee S et al (2017) Distinguishing dynamical features of water inside protein hydration layer: distribution reveals what is hidden behind the average. *J Chem Phys* 147:024901
64. Nakanishi M, Sokolov AP (2015) Protein dynamics in a broad frequency range: dielectric spectroscopy studies. *J Non-Cryst Solids* 407:478–485
65. Nandi N, Bagchi B (1997) Dielectric relaxation of biological water. *J Phys Chem* 101:10954–10961
66. Nandi N et al (2000) Dielectric relaxation and solvation dynamics of water in complex chemical and biological systems. *Chem Rev* 100(6):2013–2046
67. Nibali VC (2020) Wrapping up hydrophobic hydration: locality matters. *J Phys Chem Lett* 11:4809–4816
68. Oleinikova A et al (2004) What can really be learned from dielectric spectroscopy of protein solutions? A case study of ribonuclease A. *J Phys Chem B* 108:8467–8474
69. Persson F et al (2018) The geometry of protein hydration. *J Chem Phys* 148(21):215101
70. Pattni V et al (2017) Distinct protein hydration water species defined by spatially resolved spectra of intermolecular vibrations. *J Phys Chem B* 121(31):7431–7442
71. Pethig R, Kell DB (1987) The passive electrical properties of biological systems: their significance in physiology, biophysics and biotechnology. *Phys Med Biol* 32(8):933–970
72. Pethig R (1992) Protein-water interactions determined by dielectric methods. *Annu Rev Phys Chem* 43:177–205
73. Peyman A et al (2015) Variation in dielectric properties due to pathological changes in human liver. *Bioelectromagnetics* 36(8):603–612
74. Raschke TM (2006) Water structure and interactions with protein surfaces. *Curr Opin Struct Biol* 16:152–159
75. Russo D et al (2004) Hydration dynamics near a model protein surface. *Biophys J* 86:1852–1862
76. Said T, Varadan V (2009) The role of the concentration and distribution of water in the complex permittivity of breast fat tissue. *Bioelectromagnetics* 30(8):669–677
77. Sato ET et al (2015) Molecular model for hydrated biological tissues. *Phys Rev E* 91(6):063310
78. Scheider W et al (1976) Changes in the electric dipole vector of human serum albumin due to complexing with fatty acids. *Biophys J* 16:417–431
79. Schepps JL, Foster KR (1980) The UHF and microwave dielectric properties of normal and tumour tissues: variation in dielectric properties with tissue water content. *Phys Med Biol* 25:1149–1159
80. Schrieber R et al (2007) *Gelatine handbook. theory and industrial practice*. WILEY-VCH Verlag GmbH & Co. KGaA, Weinheim, pp 45–117
81. Shah NJ et al (2022) A novel MRI-based quantitative water content atlas of the human brain. *NeuroImage* 252:1–13
82. Sihvola A (2000) Mixing rules with complex dielectric coefficients. *Subsurf Sens Technol Appl* 1(4):393–415
83. Smith SR, Foster KR (1985) Dielectric properties of low-water-content tissues. *Phys Med Biol* 30(9):965–973
84. Sorushanova A et al (2019) The collagen suprafamily: from biosynthesis to advanced biomaterial development. *Adv Mater* 31(1):1801651
85. Sterpone F et al (2012) Magnitude and molecular origin of water slowdown next to a protein. *J Am Chem Soc* 134:4116–4119
86. Tang Y et al (2020) Noninvasive detection of extracellular pH in human benign and malignant liver tumors using CEST MRI. *Front Oncol* 578985:2–10
87. Villano D et al (2021) A fast multislice sequence for 3D MRI-CEST pH imaging. *Magn Reson Med* 85:1335–1349
88. Williams MA et al (1994) Buried waters and internal cavities in monomeric proteins. *Protein Sci* 3(8):1224–1235
89. Wolf M et al (2012) Relaxation dynamics of a protein solution investigated by dielectric spectroscopy. *Biochim Biophys Acta* 1824(5):723–730
90. Yamaoka K et al (1989) Reversing-pulse electric birefringence as applied to thermal denaturation of acid-soluble calf skin collagen. *Polym J* 21(1):107–109
91. Zu Z et al (2018) Spin-lock imaging of exogenous exchange-based contrast agents to assess tissue pH. *Magn Reson Med* 79(1):298–305

Publisher's Note

Springer Nature remains neutral with regard to jurisdictional claims in published maps and institutional affiliations.

Submit your manuscript to a SpringerOpen[®] journal and benefit from:

- Convenient online submission
- Rigorous peer review
- Open access: articles freely available online
- High visibility within the field
- Retaining the copyright to your article

Submit your next manuscript at ► [springeropen.com](https://www.springeropen.com)
